Serial In Vivo Imaging of the Lung Metastases Model and Gene Therapy Using HSV1-tk and Ganciclovir

Win-Ping Deng*[1], Cheng-Chia Wu*[1], Chien-Chih Lee[1], Wen K. Yang[2], Hsin-Ell Wang[3], Ren-Shyan Liu[4], Hon-Jian Wei[1], Juri G. Gelovani[5], Jeng-Jong Hwang[3], Den-Mei Yang[2], Ying-Kai Fu[6], and Cheng-Wen Wu[7]

[1]Graduate Institute of Biomedical Materials, Taipei Medical University, Taipei, Taiwan; [2]Laboratory of Cell/Gene Therapy, China Medical University Hospital, Taichung, Taiwan; [3]Institute of Radiological Science, National Yang-Ming University, Taipei, Taiwan; [4]Department of Nuclear Medicine and National PET Cyclotron Center, Veterans General Hospital, Taipei, Taiwan; [5]Department of Experimental Diagnostic Imaging, M.D. Anderson Cancer Center, Houston, Texas; [6]Institute of Nuclear Energy Research, Taoyuan, Taiwan; and [7]National Health Research Institutes, Taipei, Taiwan

Noninvasive imaging in lung metastatic tumor models is used infrequently because of technical limitations in detecting metastases. We have previously used 2′-fluoro-2′-deoxy-5-iodo-1-β-D-arabinofuranosyluracil labeled with ^{131}I (^{131}I-FIAU) and demonstrated the applicability of noninvasive imaging for monitoring cancer gene therapy in an experimental animal model of herpes simplex virus type 1 thymidine kinase (HSV1-tk)–expressing tumor xenografts. We have now used the same animal model to effectively and noninvasively monitor the location, magnitude, and duration of therapeutic gene expression over time for the lung metastases model. **Methods:** To improve the detectability of lung metastases, an experimental blood-borne lung metastases model in mice was established using intravenously administered HSV1-tk–expressing NG4TL4 fibrosarcoma cells (NG4TL4-TK) and simulated the clinical application of HSV1-tk plus ganciclovir (GCV) prodrug activation gene therapy. The efficacy of noninvasively monitoring the sites of development of lung metastatic lesions and their GCV-induced regression were assessed by SPECT with ^{131}I-FIAU. **Results:** The results of this study showed that the lung metastases model of NG4TL4-TK cells could be successfully detected as early as 24 h after intravenous injection of tumor cells radiolabeled with ^{131}I-FIAU and also subsequently detected by extended monitoring with the intravenous injection of ^{131}I-FIAU on day 10. In mice treated with GCV, γ-camera imaging demonstrated a significant growth inhibition of NG4TL4-TK cells of primary tumors and lung metastases on day 7 after initiating treatment. **Conclusion:** We conclude that this in vivo imaging approach will be useful for future studies of the lung metastases model and for the assessment of novel anticancer and antimetastatic therapies.

Key Words: lung metastases model; ^{131}I-FIAU; noninvasive imaging; gene therapy; herpes simplex virus thymidine kinase; ganciclovir; reporter gene

J Nucl Med 2006; 47:877–884

Metastasis to the lung is a lethal attribute of sarcomas and several other cancers. Many attempts to eradicate cancer through conventional therapy (irradiation or chemotherapy) are ineffective because of treatment resistance (1–3). Currently, new promising therapies for cancer metastases have fallen behind expectations, primarily because of few available animal models and technical limitations in noninvasively detecting metastases (4). Gene therapy has been suggested as an alternative approach to battling metastases. Differing from traditional therapies, gene therapy has the potential to be more tumor specific in targeting and to selectively eradicate tumor cells with therapeutic gene expression (5). However, obstacles in cancer gene therapy are limited by the poor capacity of gene delivery, the inability to homogeneously transfect every tumor cell, and the lack of tumor-specific gene expression (2,5). To further explore the potential of gene therapy of lung metastases, a proper animal model needs to be developed to effectively and noninvasively monitor the location, magnitude, and duration of therapeutic gene expression over time.

Several attempts to optimize the methods for monitoring lung metastases include bioluminescence imaging of luciferase-expressing HT-1080 cancer cells (4), fluorescence imaging of green fluorescent protein (GFP)–expressing HT-1080 fibrosarcoma cells (1), and imaging of Na$^+$/I$^-$ symporter (NIS)–expressing pulmonary tumor with PET (6). However, applying nuclear imaging of herpes simplex virus type I thymidine kinase (HSV1-tk) gene–expressing tumor cells in a lung metastases model has not been explored. In HSV1-tk–expressing cells, the nucleoside analog 2′-fluoro-2′-deoxy-5-iodo-1-β-D-arabinofuranosyluracil labeled with ^{131}I (^{131}I-FIAU) is phosphorylated by the HSV1-TK enzyme. The ^{131}I-FIAU–monophosphate cannot cross the cellular membrane and is metabolically entrapped (7). The accumulated intracellular radioactivity allows for in vivo detection of HSV1-tk–expressing tissues by γ-camera

imaging or SPECT (8). We have previously used ^{131}I-FIAU and showed the applicability of noninvasive imaging for monitoring cancer gene therapy in an experimental animal model of HSV1-tk–expressing tumor xenografts (9,10). The HSV1-tk–expressing tumor cells become sensitive to ganciclovir (GCV), which is also phosphorylated by the HSV1-TK enzyme to monophosphate- and then by cellular kinase to diphosphate- and triphosphate-GCV. Its incorporation into DNA in proliferating tumor cells can terminate the DNA chain, ultimately triggering apoptotic death (11,12). Because HSV1-tk gene cannot be efficiently delivered and expressed homogeneously in a heterogeneous tumor tissue, this approach relies on the so-called "bystander effect," which is mediated by an exchange of GCV-triphosphate and proapoptotic signals between the HSV1-tk–expressing and neighboring nonexpressing cells (10,13–16). Distantly located cells that are devoid of HSV1-tk are not affected (17). Therefore, the HSV1-tk gene can be used as both a therapeutic gene and a reporter gene for noninvasive imaging of the location, magnitude, and duration of gene expression.

The intent of the present studies was to establish an experimental blood-borne lung metastases model in mice receiving intravenous HSV1-tk–expressing NG4TL4 fibrosarcoma cells (NG4TL4-TK). This model has the potential of future clinical application of HSV1-tk plus GCV prodrug activation gene therapy while monitoring the sites of development of lung metastatic lesions and their GCV-induced regression by noninvasive SPECT with ^{131}I-FIAU.

MATERIALS AND METHODS

Preparation of Labeled 2′-Fluoro-2′-Deoxy-1-β-D-Arabinofuranosyl-5-Iodouracil

^{131}I-Labeled NaI, without carrier, was purchased from NEN Life Services Products. No-carrier-added ^{131}I-FIAU was prepared as described (9).

Cellular Uptake of ^{131}I-FIAU

Two murine cell lines (NG4TL4 [HSV1-tk$^-$] and NG4TL4-TK [HSV1-tk$^+$]), lung-colonizing metastatic sarcoma cells, were cultured in minimum essential medium supplemented with 10% fetal bovine serum, 100 units/mL penicillin, 10 μg/mL streptomycin, and 2 mmol/L L-glutamine in a humidified atmosphere with 5% CO_2 at 37°C as described (9). We transduced the NG4TL4-TK cell line from the parental NG4TL4 fibrosarcoma cell (18) by transfecting with packaged virions of a bicistronic retroviral vector containing HSV1-tk gene.

For the cellular uptake assay, NG4TL4-TK cells were trypsinized and grown overnight in 24-well culture plate (10^5 cells/0.5 mL per well). The culture medium was changed before the experiment. The HSV1-tk–expressing NG4TL4-TK cells were incubated with ^{131}I-FIAU at ^{131}I activity concentrations of 18.5, 37, 185, 370, and 740 kBq/mL in a total volume of 0.5 mL at 37°C for 2, 4, 8, and 16 h; the parental NG4TL4 cells were likewise incubated at an ^{131}I activity concentration of 37 kBq/mL. Cells were then centrifuged and washed twice. The isolated cells, the pooled medium, and the washes were then counted separately by

γ-counting in a model 1470 Wizard γ-counter (Wallac). Triplicate measurements of radiotracer uptake were performed for each time point. The activity concentration in cells was expressed as the accumulation ratio—that is, counts per minute per gram (cpm/g) of cells divided by the cpm/g (or mL) of medium.

Survival Assay

Clonogenic survival assays were performed for cell killing induced by ^{131}I-FIAU. The NG4TL4-TK cells were seeded into 24-well culture plates with medium containing ^{131}I-FIAU at various concentrations (0, 18.5, 37, 185, 370, 740, and 1,480 kBq/mL culture medium) for 2, 4, 8, and 16 h. Cells from each condition were then plated onto 10-cm plates (300 cells/plate) in triplicates. After 10 d of growth in vitro, the surviving colonies were fixed and stained with crystal violet.

Biodistribution of ^{131}I-FIAU–Labeled NG4TL4-TK Cells

The animal experiment protocol was approved by the Institutional Animal Care and Use Committee of Taipei Medical University. Syngeneic female FVB/N inbred strain mice ($n = 3$) were injected through the tail vein with 1×10^6 NG4TL4-TK cells labeled with ^{131}I-FIAU, which were incubated with medium containing 18.5 kBq/mL ^{131}I-FIAU for 8 h before injection. The culture condition was derived from the results of cell uptake and the survival assay. Mice were killed 4 d later. Different organs and tissues were sampled, washed, weighed, and assessed for radioactivity concentration along with injection dose standards using a model 1470 Wizard γ-counter (Wallac).

Lung Morphometry and Histology

Mice were killed after the injection of 1×10^5 NG4TL4-TK cells on 7, 14, and 21 d ($n = 3$). To assess the metastatic burden in lungs, whole lungs were measured for their volume by the water displacement method and expressed by the ratio of the lung volume to the body weight; the weight of whole lungs was also measured and expressed by the ratio of the lung weight to the body weight. Thereafter, lungs were fixed in 4% paraformaldehyde and embedded in paraffin. Sections (10 μm) were cut and stained with hematoxylin and eosin (H&E.). Fourteen days after cell injection, the heart, liver, stomach, small intestine, and colon were also sampled, sectioned, and stained with H&E.

Planar Imaging and Autoradiography

Planar imaging was performed as described (9). Briefly, 1×10^6 NG4TL4-TK cells labeled with ^{131}I-FIAU, by 8-h incubation with medium containing 18.5 kBq/mL ^{131}I-FIAU, were injected into the FVB/N female mice through the tail vein ($n = 6$) to evaluate the migration of lung-colonizing metastatic sarcoma cells in the lung. Static images were obtained from anesthetized animals at 2, 4, and 24 h and on day 3, 4, and 9 with a digital γ-camera (Elscint SP-6), equipped with a high-energy pinhole collimator, a 364-keV $\pm$ 10% ^{131}I photopeak energy window, and a $256 \times 256 \times 16$ bit image matrix (19,20). On day 10, 3.7 MBq of ^{131}I-FIAU were injected into the tail vein 24 h before planar imaging to examine the possibility of long-term monitoring of NG4TL4-TK cell–induced lung metastatic tumor. Autoradiography was performed immediately afterward. The image acquisition was performed at 100 kilocounts per frame on day 1. Subsequent images were acquired by a preset-time acquisition mode.

Total RNA Extraction and Reverse Transcription Polymerase Chain Reaction (RT-PCR)

Mice were killed on day 15 and lungs were removed. First, lungs were digested with 20 mL of an enzymatic mixture containing 40 mg collagenase (Sigma-Aldrich), 40 mg hyaluronidase (Sigma-Aldrich), and 250 mg trypsin (Invitrogen) at 37°C for 1 h. RNA was extracted using TRIzol Reagent (Invitrogen). The RNA was then reverse transcribed and amplified by using Superscript III System for RT-PCR (Invitrogen). Briefly, extracted RNA was mixed with double distilled H_2O, 10× PCR buffer, 25 mmol/L $MgCl_2$, 2.5 mmol/L deoxyribonucleoside triphosphate, Taq polymerase, and primers (TK1: 5′-TGC AGC GAC CCG CTT AAC AGC GT-3′ and TK2: 5′-CAT AGA TCT GGA TCC TTC CGG TAT TGT CT-3′). Initial denaturation at 95°C for 5 min was followed by 35 thermal cycles: (a) denaturation at 94°C for 1 min; (b) annealing at 55°C for 1 min; (c) extension at 72°C for 1 min. After the 35 cycles, final extension occurred at 72°C for 5 min. In addition, reduced glyceraldehyde-phosphate dehydrogenase (GAPDH) messenger RNA was used as the standard. Primers used for GAPDH were G1 (5′-GCT CTC CAG AAC ATC ATC CCT GCC-3′) and G2 (5′-CGT TGT CAT ACC AGG AAA TGA GCT T-3′).

GCV Therapy

The 5×10^5 NG4TL4-TK cells were in vitro labeled with ^{131}I-FIAU by 8-h incubation with medium containing 18.5 kBq/mL ^{131}I-FIAU. Planar imaging of FVB/N female mice ($n = 6$) was performed 24 h after injection of the ^{131}I-FIAU–labeled NG4TL4-TK cells via tail vein (day 1). Fourteen days later, 3.7 MBq of ^{131}I-FIAU were injected in the tail vein 24 h before planar imaging to confirm the development of the lung metastases model. On day 15, the animals were treated with GCV (10 mg/kg daily) or with 0.09% NaCl (as a control) by intraperitoneal injection for 7 consecutive days. On day 21 (GCV-7 d), 3.7 MBq of ^{131}I-FIAU were injected in the tail vein 24 h before planar imaging. To diminish thyroid uptake of the liberated ^{131}I resulting from GCV therapy, mice were pretreated with 0.5 mL 0.9% NaI solution by intraperitoneum 15 min before ^{131}I-FIAU injection. Mice were killed on day 21 after planar imaging.

RESULTS

Survival Assay of NG4TL4-TK Cells After Cellular Uptake of ^{131}I-FIAU

These studies were conducted to evaluate the biologic effects (potential radiotoxicity), resulting from the accumulation and retention of ^{131}I-FIAU in NG4TL4-TK cells. The ^{131}I-FIAU was rapidly and selectively accumulated by the NG4TL4-TK cells; however, the magnitude of accumulation was inversely related to the increased activity concentration (Fig. 1A). The NG4TL4 (HSV1-tk negative) cells showed no significant uptake of ^{131}I-FIAU. The maximal uptake of ^{131}I-FIAU in NG4TL4-TK cells was in culture with 18.5 kBq/mL ^{131}I-FIAU for 8 h. As shown in Figure 1B, these results were supported by clonogenic survival data, where the most optimal conditions for radiolabeling of NG4TL4-TK cells was 18.5 kBq/mL ^{131}I-FIAU for 8 h, and the colony-forming efficiency was 60% ($n = 3$).
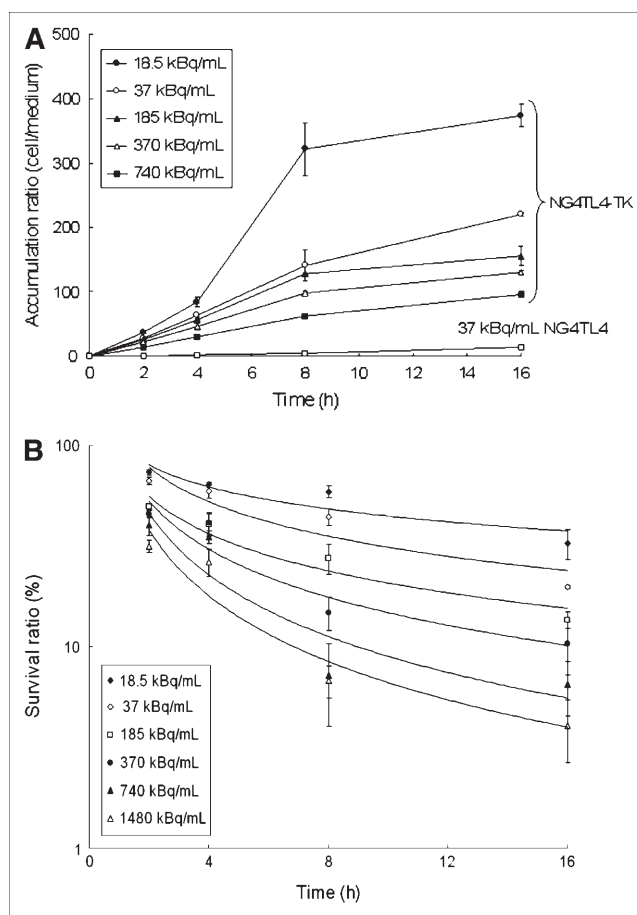

FIGURE 1. In vitro analyses of ^{131}I-FIAU-labeled NG4TL4-TK cells. (A) Cellular uptake of ^{131}I-FIAU is time dependent in HSV1-tk–transduced NG4TL4 cells (HSV1-tk[+]) but not in parental NG4TL4 cells (HSV1-tk[−]). Uptake activity is expressed as an accumulation ratio: cpm/g cells divided by cpm/g (or mL) of medium. (B) Time-dependent survival ratio of NG4TL4-TK labeled with ^{131}I-FIAU in vitro. Survival ratio was determined by using colony formation to compare the number of surviving colonies of NG4TL4-TK incubated with or without ^{131}I-FIAU for various times.

Tail Vein-Injected NG4TL4-TK Cells Efficiently Form Lung Metastases Model

To investigate whether the NG4TL4-TK cells migrate to the lungs and form the metastases model in the lungs, 10^5 cells were injected into mice through the tail vein. Mice were sacrificed and lungs were extracted 0, 7, 14, and 21 d after injection. Morphologic (Fig. 2A) and histologic (Fig. 2B) analyses of the lung tissue showed that the NG4TL4-TK cells migrate efficiently into the lungs and time dependently form metastatic lesions after injection. Tumor cells dominate the majority of the lung tissue and were observed 21 d after injection (Fig. 2B) in metastatic lesions central necrosis. As shown in Figure 2C, the histologic analysis also demonstrated that NG4TL4-TK cells preferentially metastasized to the lung but not to the colon, small intestine, stomach, liver, and heart.
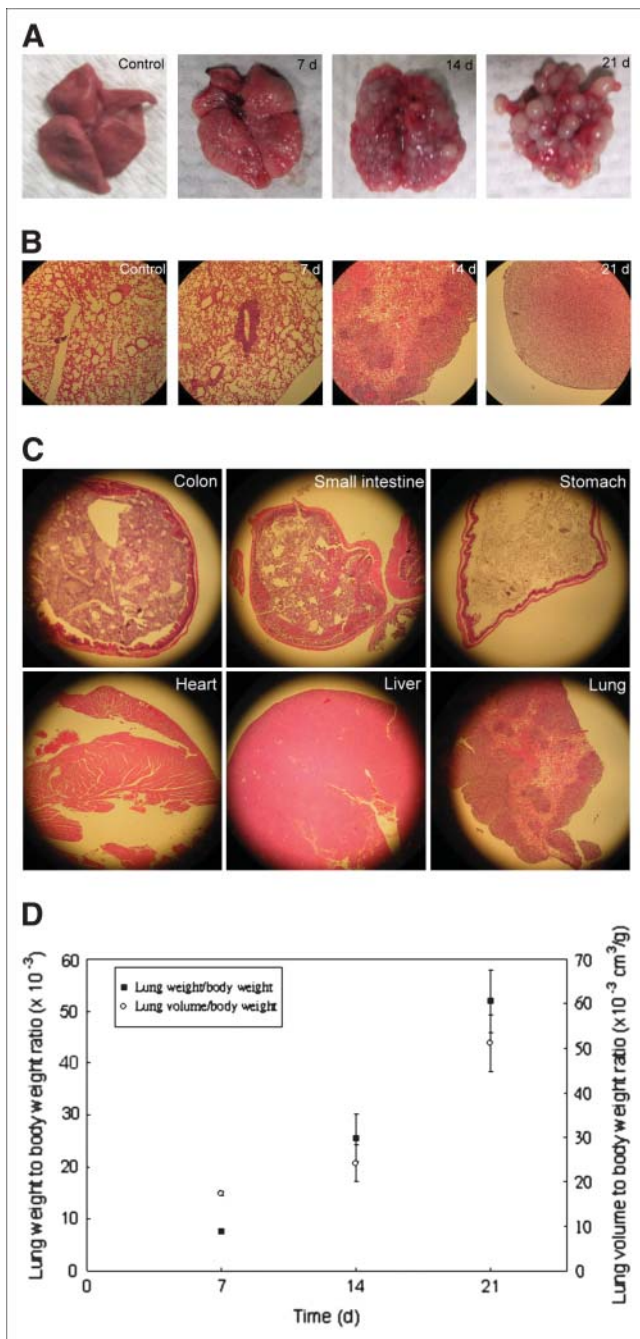
FIGURE 2. NG4TL4-TK cells migrate specifically and efficiently to lungs and form metastatic lesions. (A) Control group lungs were extracted from mice that did not receive NG4TL4-TK cells, and metastatic group lungs were extracted 7, 14, and 21 d after mice received NG4TL4-TK cells. (B) Histologic analysis of lung tissue with H&E staining: control group, NG4TL4-TK injection for 7, 14, and 21 d. (C) Sections of colon, small intestine, stomach, heart, and liver stained with H&E to confirm that NG4TL4-TK cells preferentially metastasized to lung. (D) Analyses of weight and volume of extracted lungs from mice for 7, 14, and 21 d after injection with NG4TL4-TK cells.

Lungs extracted from day 7, 14, and 21 showed an increase in both mass and volume (Fig. 2D), with the weight and volume of lung increasing dramatically after day 14. The increases of lung weight and volume were closely correlated with the increased lung tumor metastases on 7, 14, and 21 d after injection (Fig. 2A).

Serial In Vivo Imaging of ^{131}I-FIAU–Labeled NG4TL4-TK Cells for Monitoring Lung Metastases Model

After tail vein injection of ^{131}I-FIAU–labeled NG4TL4-TK cells into mice, planar imaging obtained 2 and 4 h after injection showed radiolabeled cell–derived radioactivity in the blood pool (Fig. 3A). Twenty-four hours later, strong activity was clearly visible in the area of the lungs, but no substantial activity was found in any other area of the body. This initially detected activity in the lungs gradually decayed on day 3 and 4. By day 9, residual blood-borne and lung activities had cleared.

To examine the possibility of long-term monitoring of NG4TL4-TK cell–derived lung metastatic tumor lesions, 3.7 MBq of ^{131}I-FIAU were readministered on day 10. Planar imaging clearly demonstrated the presence of NG4TL4-TK cells in lung metastatic tumor lesions but not in the control group (Fig. 3A, 10 d). Thereafter, the mice were killed and autoradiography was performed in whole-body section, showing lungs containing NG4TL4-TK cell–induced metastatic tumor lesions. Nonspecific uptake in the thyroid and the bladder was also observed on planar imaging and on autoradiography. The expression of HSV1-tk gene in lungs with NG4TL4-TK cell–derived metastatic tumor lesions was confirmed by RT-PCR analysis (Fig. 3B).

Table 1 shows the quantitative tissue distribution of ^{131}I-FIAU–labeled NG4TL4-TK cells in FVB/N mice, indicating the preferential localization of macroscopic NG4TL4-TK cell–derived metastatic tumor lesions in lungs as compared with other tissues ($P < 0.01$).

Tumor Regression and Planar γ-Imaging Studies

These studies were conducted to examine the effectiveness of the prodrug activation therapy in NG4TL4-TK cell–induced lung metastatic tumor lesions. First, the mice were injected with ^{131}I-FIAU–labeled NG4TL4-TK cells and imaged with the γ-camera to verify the metastatic lesion burden in the lungs. Planar imaging showed that the NG4TL4-TK cells migrated to the lungs within 1 d (Fig. 4A, 1 d). After 14 d, readministeration of ^{131}I-FIAU via the tail vein confirmed the NG4TL4-TK cells' metastatic development in lungs (Fig. 4A, 14 d [GCV-0 d]). Because the readministration of ^{131}I-FIAU in Figure 3A on day 10 showed strong uptake of ^{131}I in the thyroid, mice were treated with 0.9% NaI by intraperitoneal injection 15 min before ^{131}I-FIAU injection to eliminate the thyroid background. After having received GCV for 7 d, the metastatic burden was significantly diminished (Fig. 4A, 21 d [GCV-7 d]), as manifested by lower ^{131}I-FAIU–derived signal intensity, than in the untreated mice (Fig. 4A, 21 d [Control]).
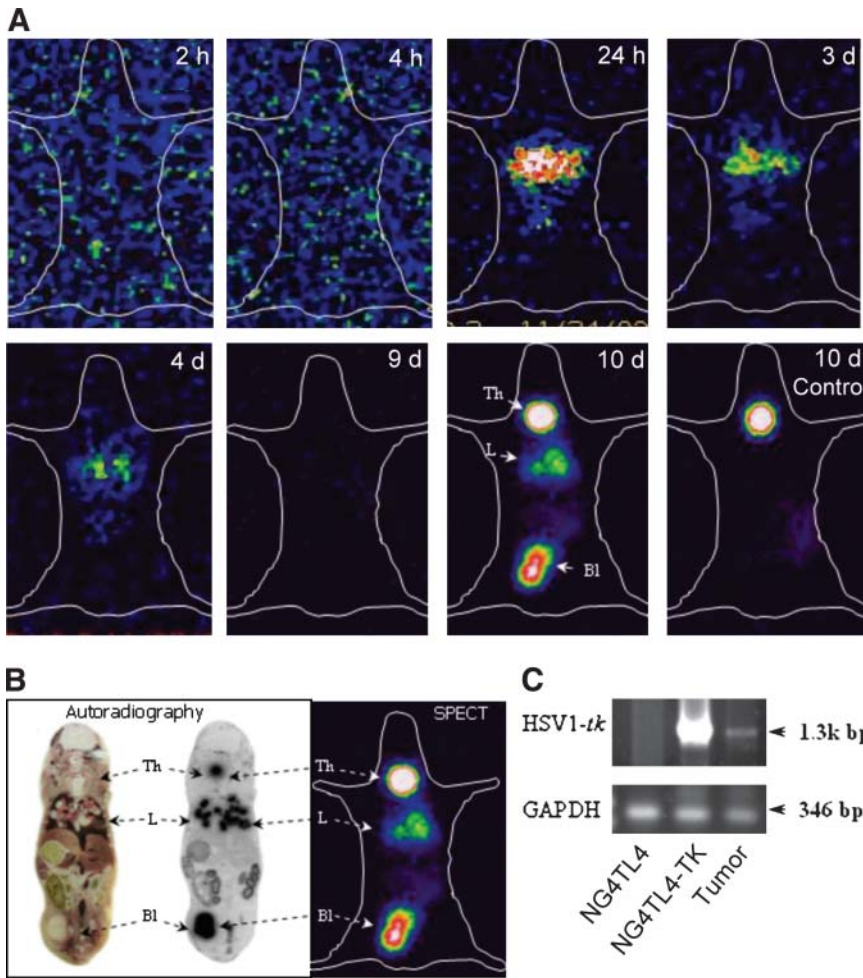
FIGURE 3. Serial in vivo imaging of migration and targeting of ^{131}I-FIAU–labeled NG4TL4-TK cells, lung-colonizing metastatic sarcoma cells, in FVB/N mice. (A) Representative serial planar γ-camera imaging of syngeneic FVB/N inbred strain mice ($n = 6$) at 2, 4, and 24 h and on 3, 4, and 9 d after tail vein injection of 1×10^6 NG4TL4-TK cells labeled with ^{131}I-FIAU. On day 10, ^{131}I-FIAU was readministered through the tail vein for long-term monitoring of NG4TL4-TK cell–induced lung metastatic tumor lesions. Imaging of lung was not evident in control group on day 10. (B) Autoradiogram of ^{131}I in 10-μm-thick whole-body section. Dark areas on autoradiogram correspond to areas of high γ-detection from radiolabeled tumor via SPECT. (C) RT-PCR detection of HSV1-tk expression in cells extracted from NG4TL4-TK cell–derived metastatic lung tumor lesions. GAPDH was used as standard. Th = thyroid; L = lung; Bl = bladder; bp = base pairs.

This finding was supported by morphologic analysis, which showed that in the GCV treatment group (Fig. 4B, +GCV) lungs had better perfusion while having fewer growing metastatic lesions. Lungs from the control group treated with only 0.09% NaCl (Fig. 4B, −GCV) had more growing metastatic lesions and poor lung perfusion.

DISCUSSION

Creating the animal model for studies of the lung metastatic process would help greatly in evaluation of many treatments, including various gene therapies. In our previous studies (9,10), we have used ^{131}I-FIAU and demonstrated the application of noninvasive γ-camera imaging to monitor cancer gene therapy in an experimental animal model of HSV1-tk–expressing tumor cells. Using serial γ-camera imaging with ^{131}I-FIAU in this study, we have in vivo monitored noninvasively the development and GCV-induced regression of the HSV1-tk–expressing fibrosarcoma lung metastases model in mice. Current gene delivery systems cannot accomplish the effective and uniform transfection of a therapeutic gene into a heterogeneous tumor tissue (17). Hence, to adequately model and understand the in vivo heterogeneity, a polyclonal population of retrovirally transduced NG4TL4-TK cells was used. As shown in Figure 4, the efficacy of GCV-induced therapy on the lung metastases model of HSV1-tk–expressing fibrosarcomas in our study is in agreement with the results of Nagamachi et al. (21) and Shibata et al. (22). Both teams of investigators showed that liposome-mediated transfer and in vivo electroporation of HSV1-tk to lung metastases followed by GCV treatment were effective in controlling the growth of multiple metastatic lesions. Recently, Garcia-Castro et al. (23) established the paradigm of using tumor cells as cellular vehicles to deliver gene therapies to metastatic tumor growth.

In our study, we found that the use of a serial planar γ-camera could detect cellular migration to the lungs 24 h after injection and that extended monitoring with the intravenous reinjection of ^{131}I-FIAU also detected lung metastases on day 10 (Fig. 3). On the basis of these findings, we suggest that the application of SPECT may be applicable for imaging the heterogeneity of transgene expression in targeted tumor metastases (20). The use of serial in vivo γ-camera imaging with ^{131}I-FIAU of the lung metastases model in HSV1-tk–expressing tumors has 2 advantages: (a) ^{131}I has a half-life of 8 d. This characteristic will allow in vitro labeling of tumor cells for highly specific

Tissue distribution	n	Activity (%ID/g)*
Blood	3	0.036 ± 0.023
Brain	3	0.029 ± 0.018
Thyroid	3	0.685 ± 0.338
Lung	3	87.1 ± 24.9
Heart	3	0.025 ± 0.011
Stomach	3	0.967 ± 0.558
Liver	3	0.536 ± 0.312
Spleen	3	0.069 ± 0.038
Large intestine	3	0.841 ± 0.361
Small intestine	3	4.97 ± 2.11
Kidney	3	0.138 ± 0.023
Bladder	3	0.008 ± 0.003
Muscle	3	0.044 ± 0.011
Bone	3	0.036 ± 0.019
Abdominal fat	3	0.164 ± 0.068

*Percentage injected dose per gram of tissue at 4 d after tail vein injection of 1×10^6 NG4TL4-TK cells labeled with ^{131}I-FIAU, corrected for radioactive decay to time of injection.

Data are expressed as mean ± SEM.

imaging of cellular trafficking with lower background from the radiotracer biodistribution and clearance; and (b) FIAU can be radiolabeled with several radioisotopes of iodine suitable for γ-camera (^{123}I, ^{125}I, ^{131}I) or PET ([124]I), allowing the use of different radionuclide imaging modalities. For example, Koehne et al. (20) showed that HSV1-tk transfected T-lymphocytes can be efficiently radiolabeled with ^{131}I-FIAU ex vivo (in vitro) to monitor cellular migration in vivo after intravenous administration in mice and, furthermore, that the use of repetitive PET with intravenously administered [124]I-FIAU could trace the fate of intravenously administered nonlabeled HSV1-tk transfected T-lymphocytes.

PET may be the preferable imaging system for monitoring gene expression because of its superior sensitivity and properties for quantification of regional tracer accumulation (24). To monitor the fate of lung metastatic tumor continuously, the ^{131}I-FIAU was readministrated via the tail vein into the mice bearing lung tumor, and the imaging showed a strong uptake of ^{131}I in the thyroid glands (Fig. 3A, 10 d). For planar imaging, we found in this study that showing thyroid uptake could help confirm the position of the lung metastatic tumor. To obtain clearer imaging in the lung metastatic tumor lesion site during GCV-induced regression, we used 0.9% NaI to eliminate the background of thyroid uptake (Fig. 4A, 14 and 21 d). The imaging in Figure 4 showed higher abdominal background than that in Figure 3 (10 d). The background can be a normal pattern of intestinal metabolic degradation (9,25) and this can be proven by the distribution of the radiotracer in normal mice (26). These results in our study are supported by the biodistribution of the mice (Fig. 4), showing that besides the HSV1-tk–expressing lung tumor, the small intestine had a much higher accumulation than other tissues (lung, 75.1%; small intestine, 15.3%; stomach, 4.5%; large intestine, 2.6%; and liver, 1.3%). The GCV-treated mice (Fig. 4A, 21 d [GCV-7 d]) also showed much higher abdominal

FIGURE 4. HSV1-tk gene therapy with GCV to eradicate metastatic tumor. (A) Planar imaging of syngeneic FVB/N mice (n = 6) bearing lung metastatic tumor induced by ^{131}I-FIAU–labeled NG4TL4-TK cells was performed 24 h after injection of cells (day 1). On day 14 (GCV-0 d) and day 21 (GCV-7 d), ^{131}I-FIAU was readministered via tail vein 24 h before planar imaging. A significant reduction in signal was evident at lungs with GCV treatment for 7 d (21 d, GCV-7 d) compared with that of control mice without GCV treatment (21 d, Control). L = lung; In = small intestine. (B) Representative lungs from treatment group (+GCV). Lungs from GCV treatment group were better vascularized with fewer metastatic nodules than lungs from control group. Lungs from control group, which received NG4TL4-TK cells but were treated with only 0.09% NaCl (−GCV), had more metastatic lesions and poor vascularization.
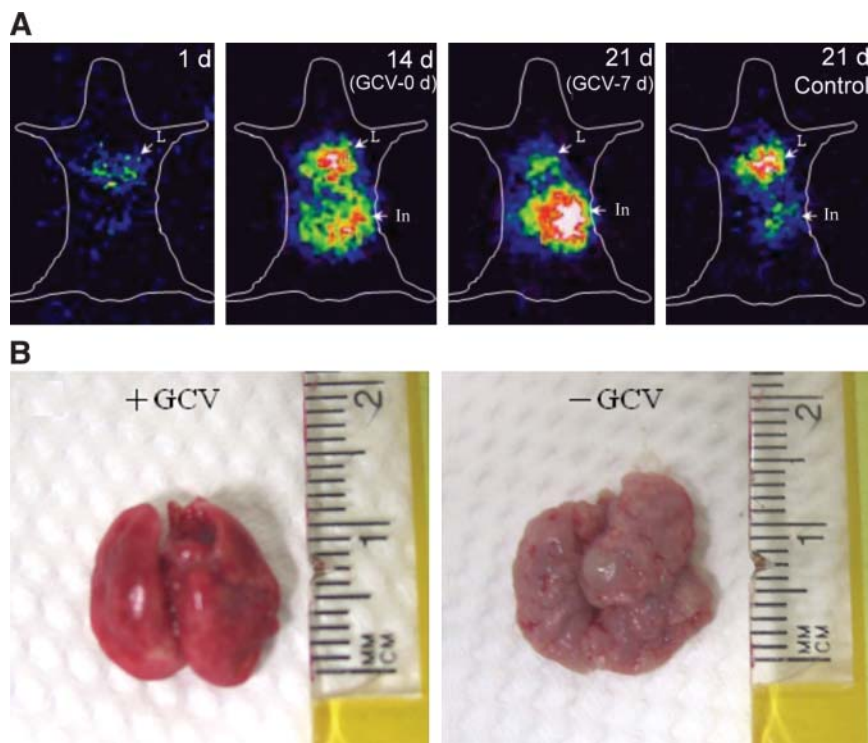
uptake than the control mice (Fig. 4A, 21 d [Control]). When GCV eliminated the HSV1-tk–expressing lung tumor cells, fewer target cells would accumulate the radiotracer (^{131}I-FIAU). Therefore, GCV-treated mice had higher abdominal uptake than the control mice because of its elimination predominantly through the intestinal route.

Previously published methods of monitoring lung metastasis include the application of real-time fluorescence imaging of GFP expression and NIS gene-mediated PET with ^{124}I. Both methods have specific limitations (1,6). Yamamoto et al. reported that while using real-time GFP imaging of lung metastasis, a skin-flap window was needed to improve resolution attributed to autofluorescence. Marsee et al. concluded that NIS-mediated PET, in comparison with HSV1-tk /FIAU reporter gene-mediated imaging, does not efficiently incorporate radioiodine into the cell structure and the isotope accumulation is only temporary (27,28).

The increasing clinical use of PET, and the preclinical applications of animal PET systems, is due to the improved spatial resolution. The spatial resolution of most clinical PET scanners for the body is around $(6–8)^3$ mm^3 and that for the brain is around 3^3 mm^3 (29). Small-animal PET scanners have been recently developed to a spatial resolution of around 2^3 mm^3 (30), but the scanners of newer generation systems will reach a resolution of around 1^3 mm^3 (31).

CONCLUSION

Applications of the HSV1-tk gene in clinical gene therapy are increasing. Several phase I clinical trails for HSV1-tk/GCV therapy on prostate cancer, gliomas (32–34), and ovarian cancer (35) have already been reported. On the basis of the results of the present study, and those described in the literature (6–9,20,25), we predict the future feasibility of using nuclear radiologic imaging to monitor the efficacy of gene delivery and expression and the future therapeutic efficacy in clinical trials on cancer gene therapy.

REFERENCES

1. Yamamoto N, Yang M, Jiang P, et al. Real-time GFP imaging of spontaneous HT-1080 fibrosarcoma lung metastases. *Clin Exp Metastasis.* 2003;20:181–185.
2. Yazawa K, Fisher WE, Brunicardi FC. Current progress in suicide gene therapy for cancer. *World J Surg.* 2002;26:783–789.
3. Cameron MD, Schmidt EE, Kerkvliet N, et al. Temporal progression of metastasis in lung: cell survival, dormancy, and location dependence of metastatic inefficiency. *Cancer Res.* 2000;60:2541–2546.
4. Nogawa M, Yuasa T, Kimura S, et al. Monitoring luciferase-labeled cancer cell growth and metastasis in different in vivo models. *Cancer Lett.* 2005;217:243–253.
5. Greco O, Dachs GU. Gene directed enzyme/prodrug therapy of cancer: historical appraisal and future prospectives. *J Cell Physiol.* 2001;187:22–36.
6. Marsee DK, Shen DH, MacDonald LR, et al. Imaging of metastatic pulmonary tumors following NIS gene transfer using single photon emission computed tomography. *Cancer Gene Ther.* 2004;11:121–127.
7. Tjuvajev JG, Chen SH, Joshi A, et al. Imaging adenoviral-mediated herpes virus thymidine kinase gene transfer and expression in vivo. *Cancer Res.* 1999;59:5186–5193.
8. Blasberg RG, Tjuvajev JG. Molecular-genetic imaging: current and future perspectives. *J Clin Invest.* 2003;111:1620–1629.
9. Deng WP, Yang WK, Lai WF, et al. Non-invasive in vivo imaging with radiolabelled FIAU for monitoring cancer gene therapy using herpes simplex virus type 1 thymidine kinase and ganciclovir. *Eur J Nucl Med Mol Imaging.* 2004;31:99–109.
10. Wei SJ, Chao Y, Shih YL, Yang DM, Hung YM, Yang WK. Involvement of Fas (CD95/APO-1) and Fas ligand in apoptosis induced by ganciclovir treatment of tumor cells transduced with herpes simplex virus thymidine kinase. *Gene Ther.* 1999;6:420–431.
11. Mar EC, Chiou JF, Cheng YC, Huang ES. Inhibition of cellular DNA polymerase alpha and human cytomegalovirus-induced DNA polymerase by the triphosphates of 9-(2-hydroxyethoxymethyl)guanine and 9-(1,3-dihydroxy-2-propoxymethyl) guanine. *J Virol.* 1985;53:776–780.
12. Ilsley DD, Lee SH, Miller WH, Kuchta RD. Acyclic guanosine analogs inhibit DNA polymerases alpha, delta, and epsilon with very different potencies and have unique mechanisms of action. *Biochemistry.* 1995;34:2504–2510.
13. Freeman SM, Abboud CN, Whartenby KA, et al. The "bystander effect": tumor regression when a fraction of the tumor mass is genetically modified. *Cancer Res.* 1993;53:5274–5283.
14. Pope IM, Poston GJ, Kinsella AR. The role of the bystander effect in suicide gene therapy. *Eur J Cancer.* 1997;33:1005–1016.
15. Samejima Y, Meruelo D. 'Bystander killing' induces apoptosis and is inhibited by forskolin. *Gene Ther.* 1995;2:50–58.
16. Wei SJ, Chao Y, Hung YM, et al. S- and G2-phase cell cycle arrests and apoptosis induced by ganciclovir in murine melanoma cells transduced with herpes simplex virus thymidine kinase. *Exp Cell Res.* 1998;241:66–75.
17. Mesnil M, Yamasaki H. Bystander effect in herpes simplex virus-thymidine kinase/ganciclovir cancer gene therapy: role of gap-junctional intercellular communication. *Cancer Res.* 2000;60:3989–3999.
18. Yang WK, Ch'ang LY, Koh CK, Myer FE, Yang MD. Mouse endogenous retroviral long-terminal-repeat (LTR) elements and environmental carcinogenesis. *Prog Nucleic Acid Res Mol Biol.* 1989;36:247–266.
19. Rosenthal MS, Cullom J, Hawkins W, Moore SC, Tsui BM, Yester M. Quantitative SPECT imaging: a review and recommendations by the Focus Committee of the Society of Nuclear Medicine Computer and Instrumentation Council. *J Nucl Med.* 1995;36:1489–1513.
20. Koehne G, Doubrovin M, Doubrovina E, et al. Serial in vivo imaging of the targeted migration of human HSV-TK-transduced antigen-specific lymphocytes. *Nat Biotechnol.* 2003;21:405–413.
21. Nagamachi Y, Tani M, Shimizu K, Yoshida T, Yokota J. Suicidal gene therapy for pleural metastasis of lung cancer by liposome-mediated transfer of herpes simplex virus thymidine kinase gene. *Cancer Gene Ther.* 1999;6:546–553.
22. Shibata MA, Morimoto J, Otsuki Y. Suppression of murine mammary carcinoma growth and metastasis by HSVtk/GCV gene therapy using in vivo electroporation. *Cancer Gene Ther.* 2002;9:16–27.
23. Garcia-Castro J, Martinez-Palacio J, Lillo R, et al. Tumor cells as cellular vehicles to deliver gene therapies to metastatic tumors. *Cancer Gene Ther.* 2005;12:341–349.
24. Haubner R, Avril N, Hantzopoulos PA, Gansbacher B, Schwaiger M. In vivo imaging of herpes simplex virus type 1 thymidine kinase gene expression: early kinetics of radiolabelled FIAU. *Eur J Nucl Med.* 2000;27:283–291.
25. Hung SC, Deng WP, Yang WK, et al. Mesenchymal stem cell targeting of microscopic tumors and tumor stroma development monitored by noninvasive in vivo positron emission tomography imaging. *Clin Cancer Res.* 2005;11:7749–7756.
26. Vaidyanathan G, Zalutsky MR. Preparation of 5-[^{131}I]iodo- and 5-[^{211}At]astato-1-(2-deoxy-2-fluoro-beta-D-arabinofuranosyl) uracil by a halodestannylation reaction. *Nucl Med Biol.* 1998;25:487–496.
27. Chung JK. Sodium iodide symporter: its role in nuclear medicine. *J Nucl Med.* 2002;43:1188–1200.
28. Dingli D, Russell SJ, Morris JC 3rd. In vivo imaging and tumor therapy with the sodium iodide symporter. *J Cell Biochem.* 2003;90:1079–1086.
29. Massoud TF, Gambhir SS. Molecular imaging in living subjects: seeing fundamental biological processes in a new light. *Genes Dev.* 2003;17:545–580.
30. Cherry SR, Gambhir SS. Use of positron emission tomography in animal research. *ILAR J.* 2001;42:219–232.

31. Chatziioannou A, Tai YC, Doshi N, Cherry SR. Detector development for microPET II: a 1 microl resolution PET scanner for small animal imaging. *Phys Med Biol.* 2001;46:2899–2910.

32. Freytag SO, Khil M, Stricker H, et al. Phase I study of replication-competent adenovirus-mediated double suicide gene therapy for the treatment of locally recurrent prostate cancer. *Cancer Res.* 2002;62:4968–4976.

33. Germano IM, Fable J, Gultekin SH, Silvers A. Adenovirus/herpes simplex-thymidine kinase/ganciclovir complex: preliminary results of a phase I trial in patients with recurrent malignant gliomas. *J Neurooncol.* 2003;65:279–289.

34. Prados MD, McDermott M, Chang SM, et al. Treatment of progressive or recurrent glioblastoma multiforme in adults with herpes simplex virus thymidine kinase gene vector-producer cells followed by intravenous ganciclovir administration: a phase I/II multi-institutional trial. *J Neurooncol.* 2003;65:269–278.

35. Hasenburg A, Fischer DC, Tong XW, et al. Histologic and immunohistochemical analysis of tissue response to adenovirus-mediated herpes simplex thymidine kinase gene therapy of ovarian cancer. *Int J Gynecol Cancer.* 2002;12:66–73.